

AERODYNAMIC ANALYSIS OF SWEEP PROPELLER WITH BET AND RANS

O. Bergmann¹, F. Möhren¹, C. Braun¹, F. Janser¹

Abstract

The primary noise source in general aviation and urban air mobility is propeller and rotor noise, which is an important annoyance factor of aviation. A feasible measure to reduce noise emissions is the application of swept propellers. It is crucial to have simulation methods of swept planforms to find an optimized propeller design. This paper presents existing and novel sweep correction models for blade element theories (BET). The correction models are compared against Reynolds-Averaged Navier Stokes (RANS) solutions for different propeller sweeps. The comparison shows a significant improvement of the BET performance prediction by applying existing correction methods and using the airfoil sections orthogonal to the local radius. The novel correction models derived from geometric planform parameters further improve the power prediction accuracy of the BET approach. The RANS and BET comparison shows that no sweep correction models are required for less swept propellers for accurate thrust and power prediction. However, the sweep correction models improve the overall performance prediction.

Keywords BET, CFD Propeller Simulation, Propeller aerodynamics, Actuator disk modelling, Propeller Performance

ACKNOWLEDGMENTS

The authors acknowledge the financial support by the Federal Ministry of Education and Research of Germany in the framework of IngenieurNachwuchs 2016 (project "DEFANA – Ducted Electric Fans for Novel Aircraft", project number 13FH638IX6). The authors like to express their gratitude to Siemens PLM Software for providing academic licenses of their software StarCCM+.

Funding

Federal Ministry of Education and Research of Germany in the framework of IngenieurNachwuchs 2016 (project "DEFANA – Ducted Electric Fans for Novel Aircraft", project number 13FH638IX6)

ABBREVIATIONS

Acronyms

| | |
|------|---------------------------------|
| BET | Blade Element Theory |
| CFD | Computational Fluid Dynamics |
| J | Advance Ratio |
| RANS | Reynolds-Averaged Navier-Stokes |

Latin

| | |
|--------------|------------------|
| C_{chord} | Chord length |
| c_d | Drag coefficient |
| c_l | Lift coefficient |
| D | Drag |
| L | Lift |
| N_{Blades} | Number of blades |
| P | Power |
| Q | Torque |
| R | Propeller Radius |
| r | Local radius |
| ρ | Density |

| | |
|-------------|---|
| T | Thrust |
| u | Circumferential velocity |
| v_∞ | Free stream velocity |
| w | Relative velocity |
| w_a | Axial velocity |
| w_t | Tangential velocity |
| Greek | |
| α | Effective angle of attack |
| β | Propeller Twist |
| η | Efficiency |
| Γ | Circulation |
| Λ_L | Local sweep angle |
| ω_p | Angular velocity |
| ϕ | Helix angle |
| ρ | Density |
| σ | Blade Solidity = $c_{chord} \cdot N_{Blades} / r_L$ |

Subscripts

| | |
|---|--------------------------------------|
| ' | Section coefficients / section loads |
| L | Local turned coordinate system |
| r | Local radius dependency |

1. INTRODUCTION

Reducing noise emissions of propeller-driven aircraft and unmanned aerial vehicles is essential for urban air mobility. Vertical take-off and landing concepts have pronounced noise constraints due to the acceptance of the inhabitants and the resistance time of hovering systems compared to conventional approaches. Especially electrically powered mobility solutions promise noise reduction possibilities by distributed propulsion, where the propeller is the primary source of noise emissions [1]. Propeller noise can be reduced by applying different measures. One feasible way to reduce the propeller noise at a fixed diameter and

number of blades, which are often defined as a top level aircraft requirements, is a sweep variation [2, 3]. Propeller noise evaluation with a computational acoustic solver needs accurate aerodynamic performance data. In preliminary design, these aerodynamic performance data can be provided by blade element theories (BET). However, classical BET cannot simulate swept propellers because of theoretical limitations. Therefore, sweep correction models are necessary to analyse swept propellers properly and to perform noise emission optimisations.

This paper provides information about the aerodynamic simulation accuracy and the limitation of BEM methods. Additionally, this paper presents novel correction methods for swept propellers in BET environments next to the existing sweep correction method. The geometric changes due to sweep are described and correction methods are derived from planform parameters.

First, the influence of propeller sweep is analysed with high fidelity Reynolds Average Navier-Stokes (RANS) simulations. A parameter variation with a generic propeller, which ensures sweep variation with otherwise unchanged geometrical properties, shows the influence of sweep as a function of the advance ratio (J). Forward and backward sweep as well as an S-shape and an unswept propeller as a baseline are analysed.

Second, the same generic propellers are analysed with a BET solver. The aeroelastic and aeroacoustic BET solver PropCODE computes the aerodynamic performance of the propeller. PropCODE - "Propeller Comprehensive Optimisation and Design Environment" is an in-house tool for aeroacoustic and aeroelastic propeller simulation and ducted propeller optimisation. PropCODE is developed in cooperation with the propeller manufacturer Helix Carbon GmbH. PropCODE, compared to other BET solvers, combines production requirements with a holistic optimisation procedure for a fast propeller design for new applications and aircraft. PropCODE processes the construction geometry automatically, generates necessary 2D airfoil polars, and performs aeroelastic and aeroacoustic computations. The link between construction file and analysis is required because due to the strong dependency between twist and chord distribution and aerodynamic performance. Minor errors in the twist distribution result in significant errors in the aerodynamic performance. For acoustic optimisation, the BET solver is extended with existing and novel sweep correction models. The aerodynamic model for straight propellers is validated in hover condition and compared with high fidelity data in Ref. [4].

The literature review shows that insufficient understanding of swept propellers in BET exists. In wind turbine applications, rotor sweep is corrected by using the well-known sweep correction approach for swept or sheared wings, according to Busemann [5]. However, in rotary applications, sweep affects the 2D airfoil parameters and normal Mach numbers and the tangential velocities, which have to be described in the local cylindrical coordinate system as it is performed by Rosen and Gur [6, 7]. We present a novel approach for swept propeller blades in BET procedures. The novel approach corrects the lift, drag, and effective direction of the tangential force.

The sweep correction models in BET are compared against high fidelity RANS solution. This paper shows general differences between swept and unswept propeller simulation approaches with BET and RANS. The swept propeller investigation and comparison identify the best aerodynamic sweep correction models for BET simulation approaches by correcting the later presented procedure stepwise.

2. NUMERICAL METHODS

The low fidelity BET results are compared against high fidelity RANS simulations. Subchapter 2.1 describes in detail the BET simulations and the multiple sweep correction models. RANS simulations are performed with the commercial CFD solver Simcenter StarCCM+. A detailed explanation of the RANS approach is presented in subchapter 2.2.

2.1. Blade Element Method

BET approaches are developed initially for straight unswept wings or propellers. The airfoils usually are staggered at the quarter chord point along a fixed axis. Staggering at the leading or trailing edge or an arbitrary point, e.g., the mid-point or the elastic axis, is also possible and doesn't affect the procedure. Tapering of the propeller is necessary for less loaded blade tips and also doesn't affect the procedure. Each airfoil behaves like an infinite wing, without tip or root effects. The flow velocities are evaluated at each 2D section, and the resulting forces are calculated according to FIGURE 1 and the following procedure.

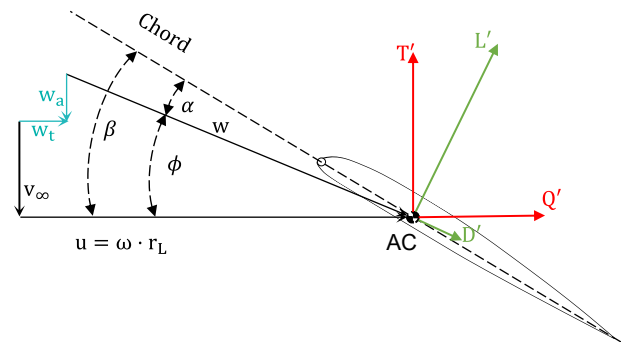


FIGURE 1: Velocities and forces at a 2D blade section

- (1)
$$L' = \frac{\rho}{2} \cdot w^2 \cdot c_l \cdot C_{\text{chord}}$$
- (2)
$$D' = \frac{\rho}{2} \cdot w^2 \cdot c_d \cdot C_{\text{chord}}$$
- (3)
$$w_a = v_{\infty} \cdot a_a$$
- (4)
$$a_a = \frac{(1 + a_a) \cdot \sigma \cdot [c_L \cos(\phi) - c_D \sin(\phi)]}{4 \sin^2(\phi)}$$
- (5)
$$w_t = u \cdot a_t$$

$$(6) \quad a_t = \frac{(1 + a_t) \cdot \sigma \cdot [c_L \sin(\phi) + c_D \cos(\phi)] \cdot v_\infty}{4 \sin^2(\phi) \cdot u}$$

$$(7) \quad F = \frac{2}{\pi} \arccos(e^{-f})$$

$$(8) \quad f = \frac{N_{Blades} \cdot R - r}{2 \cdot r \sin(\phi)}$$

$$(9) \quad T' = L' \cdot \cos(\phi) \cdot F - D' \cdot \sin(\phi)$$

$$(10) \quad Q' = L' \cdot \sin(\phi) \cdot F + D' \cdot \cos(\phi)$$

$$(11) \quad T = N_{Blades} \cdot \int_{R_{Hub}}^{R_{Tip}} T'_r \cdot dr_L$$

$$(12) \quad Q = N_{Blades} \cdot \int_{R_{Hub}}^{R_{Tip}} Q'_r \cdot r_L \cdot dr_L$$

$$(13) \quad P = Q \cdot \omega_p$$

$$(14) \quad c_T = \frac{T}{\rho A (R \omega_p)^2}$$

$$(15) \quad c_P = \frac{P}{\rho A (R \omega_p)^3}$$

With the use of the momentum equations, the induced axial w_a and tangential w_a velocities are calculated. The momentum theory is applied to ring elements for each propeller section [8]. Force equations and momentum equations are iterated and need approximately 20 iterations till convergence, starting from an induced velocity of zero. Prandtl's tip loss correction F simulates the 3D lift reduction at the propeller tip due to the vortex-induced upwash. An equivalent formulation for root losses can be included in the procedure [9].

Swept propellers require some modifications of the above-stated procedure due to the changed position of the quarter chord, and therefore changed local radial position for the same global x-position (see. FIGURE 2). The equations are still valid, but the change of the segment length and the change of twist and chord distributions have to be taken into account concerning the local radius r_L .

FIGURE 2 shows the difference between an unswept and a swept propeller blade at the same radius. The same radius results in the same rotational velocity. The rotational velocity is turned compared to the unswept propeller blade to be orthogonal to r_L and no longer orthogonal to the global x-axis, since the tangential velocity is calculated with the cross product of \vec{r}_L and $\vec{\omega}_p$. The airfoil sections are staggered along the quarter chord line, which is curved. The local airfoil at r_L has to be aligned with the tangential velocity u , which is automatically done for the unswept propeller blade on the right-hand side of FIGURE 2.

FIGURE 3 shows a closer look at the local airfoil section at r_L . With respect to r_L the local sweep Λ_L has to be defined as the angle between the tangential of the quarter chord line and r_L .

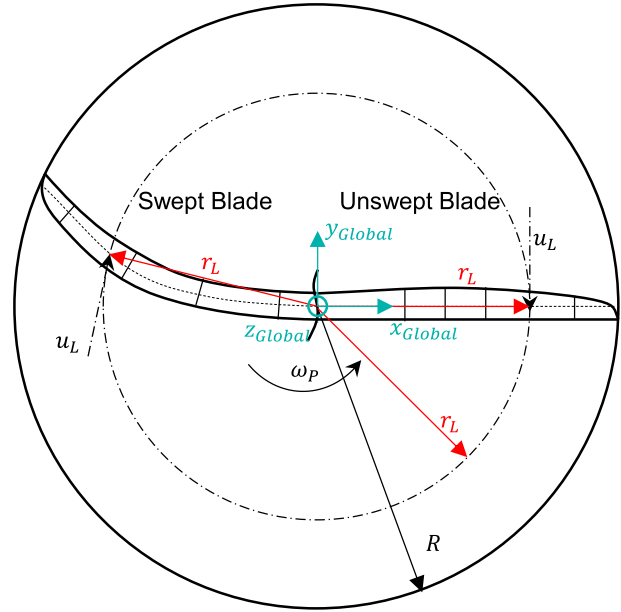


FIGURE 2: Differences between an unswept and a swept propeller blade

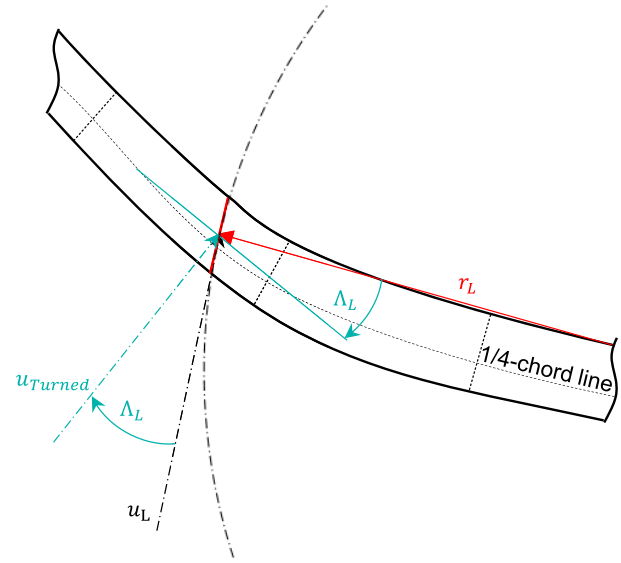


FIGURE 3: Definition of local sweep

The resulting tangential force orthogonal to r_L is required for the torque calculation, as to see in FIGURE 4. Therefore we correct the local tangential velocity u_L by turning it into the turned coordinate system normal to the local sweep u_{Turned} . Accordingly, the change of the local velocity in an orthogonal part directly affects the lift calculation in equation (1). This correction results in the well-known cosine square law for lift reduction at swept wings, according to Busemann.

$$(16) \quad u_{Turned} = u_L \cdot \cos(\Lambda_L)$$

$$(17) \quad c_{L,Corrected} = c_L \cdot \cos^2(\Lambda_L)$$

However, the drag has to be reduced if we turn and reduce

the orthogonal tangential velocity, as stated in equation (2). Additionally, we state that the resulting tangential force Q_L' appears in the local turned coordinate system. Accordingly, we must turn the force Q_L' back in the radial coordinate system, as illustrated in FIGURE 4. Therefore the force is turned back by equation (17). Finally, by integration along the r_L , we calculate the new resulting total torque.

$$(18) \quad c_{D,Corrected} = c_D \cdot \cos^2(\Lambda_L)$$

$$(19) \quad Q_r' = Q_L' \cdot \cos(\Lambda_L)$$

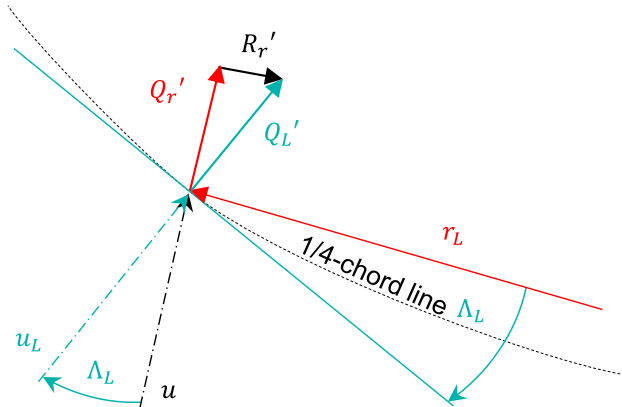


FIGURE 4: Definition of tangential force and local tangential force

The presented sweep correction models underline the difficulty of describing swept propeller blades by the basic geometric properties twist and chord distribution. It should be clear that the chord and twist distribution have to be described in the radial coordinate system because it affects the propeller's planform.

Reducing the drag due to the reduced velocity is not found in the literature. Additionally, we stated that the resulting forces act in the turned coordinate system, which is also not found in the literature. The validity of this novel approach is showed in this publication, but further validation is required.

2.2. High-fidelity propeller simulation methods

High fidelity RANS simulations are used for validation purposes of the sweep correction models in the BET procedure. The reliability of RANS prediction in propeller applications is shown in literature in multiple cases [4, 10, 11].

The High-fidelity RANS simulations are performed with the commercial software StarCCM+. A moving reference frame (MRF) approach is used to simulate the swept propeller [12]. The advantage of the MRF approach compared to other propeller simulation approaches is the fast simulation procedure for open propellers because the simulation can be performed with a steady simulation approach. Actuator disk approaches and RANS blade element approaches aren't appropriate validation sources for this kind of comparison. The RANS simulations are performed accordingly to Ref. [4]. As in Ref. [4], the boundary layer is modelled with a low y^+ approach and discretised with 25 prism layers (FIGURE 7). Approximately 75 cells are placed in chord-wise direction with further leading edge and trailing

edge refinements (FIGURE 6). Three offset meshes are generated for a smooth transition of the high resolution surface mesh to the outer flow field. The wake is further refined for a high wake resolution, which significantly affects the torque prediction. Another cylindrical volume refinement refines the volume at the blade tip. The mesh setup is presented in the following FIGURE 7.



FIGURE 5: Mesh resolution: Propeller blade

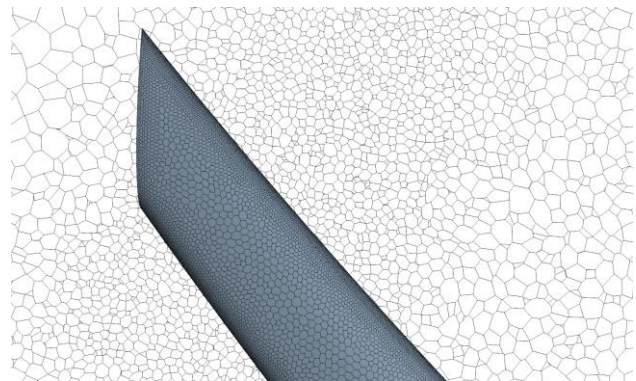


FIGURE 6: Mesh resolution: Blade tip

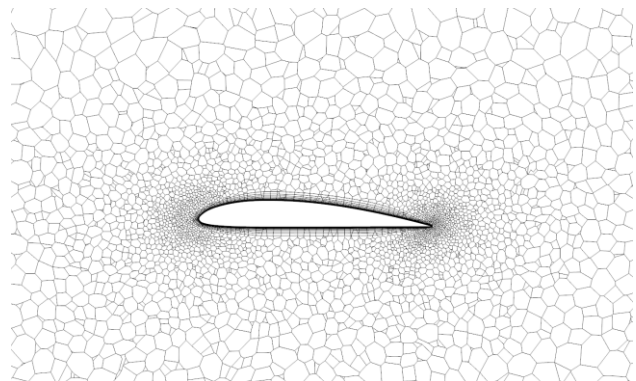


FIGURE 7: Mesh resolution: Airfoil section

The physic behaviour of the flow is solved using a coupled flow solver with the SST (Menter) $k-\omega$ turbulence model [13]. For solving the Navier-Stokes equation, an upwind scheme for the convective fluxes and a central differences scheme for the viscous fluxes are used, both 2nd order accurate. In the turbulence model, the quadratic constitutive relation scheme is used [14]. A controlled decay model guarantees a freestream turbulence viscosity ratio of 10 at the propeller [15]. Detailed information are found in Ref. [16], which summarises and gives further explanation about

the used models.

The RANS simulations are performed with 30 AMD EPYC 7742 CPU cores. Each operating point requires approximately 8 hours.

The J in the RANS simulations is stepwise increased in $\Delta J = 0.1$ steps, starting at a J of 0.1 with a constant rotational speed of 2000 1/min. Additionally, an initial simulation at an J of 0.05 is performed. The J is increased until the thrust becomes negative.

3. PROPELLER DATA

We have created a generic propeller for parameter variation. In this study, only propeller sweep is varied, while chord and twist distribution is unchanged. The airfoils are staggered at the global x-axis as defined in FIGURE 2 and not orthogonal to the local radius as required for BET calculations. They are staggered at the mid-point of the airfoils. Sweep is defined by moving the propeller tip forward and backward along the tip radius. The global sweep magnitude is expressed by a percentage global y-displacement of the propeller radius $y_{Displacement}/R_{Tip}$. Forward sweep is defined accordingly to the fixed-wing definition as negative sweep and backward sweep as positive sweep. The geometric parameters are summarised in the following table.

TABLE 1: Geometric parameter of generic Propeller

| Parameter | Value |
|------------------|--------------|
| Radius | 0.8m |
| Number of Blades | 2 |
| Airfoil | ClarkY |
| Root Chord | 90 mm |
| Taper Ratio | 0.5 |
| Root Twist | 23° |
| Tip Twist | 3° |
| Lean | 0 mm |
| Sweep | +50% to -25% |

Six different propellers are analysed, starting from a baseline without sweep. Two backward swept propellers with 25% and 50% y-displacement and one forward swept propeller with 25% y-displacement are analysed. Additionally, an s-shape propeller with backward sweep at the root and forward sweep at the tip back to 0mm tip displacement is analysed. Finally, we analysed an unconventional propeller with different twist, chord and thickness distribution as well as additional lean. The propeller has 30% backward sweep 10% lean and an increased thickness distribution by a factor of two. The following figure gives an impression of the propeller geometries.

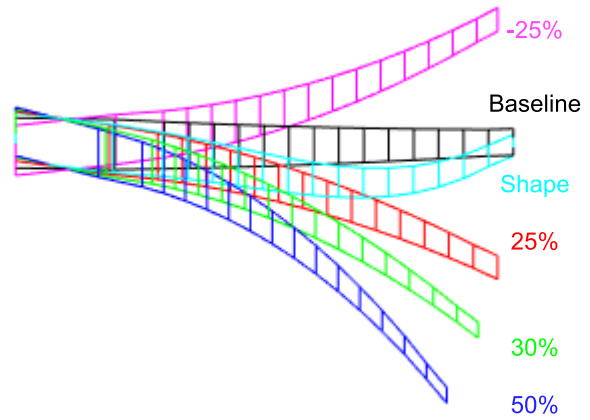


FIGURE 8: Top view: Propeller blades

The 50% swept propeller is an extremum of propeller sweep due to major bending-torion coupling effects. Therefore, this kind of propeller is an academic example for propeller sweep but should show the validity of the presented correction models.

FIGURE 9 shows the chord distribution of the airfoil sections, which are sliced orthogonal to the r_L . The sweep affects the chord length due to the turned airfoils. Increased sweep results in shorter airfoil sections. The chord length changes of the 25% forward and backward swept propellers are less than 10%, but the chord length variation increases with increased sweep. For example, the 50% swept propeller has a chord length change at the tip of 33%.

FIGURE 10 shows the corresponding twist distribution. Sweep increases the local twist, because the trailing edge twist and chord changes along the radius of the propeller. Compared to the unswept propeller, the 50% backward swept propeller has at a radius of 0.6m, 5° more twist or an increase of 40%. The propeller with 30% sweep has due to changed airfoil sections and lean a significant change in the twist distribution compared to the base line configuration.

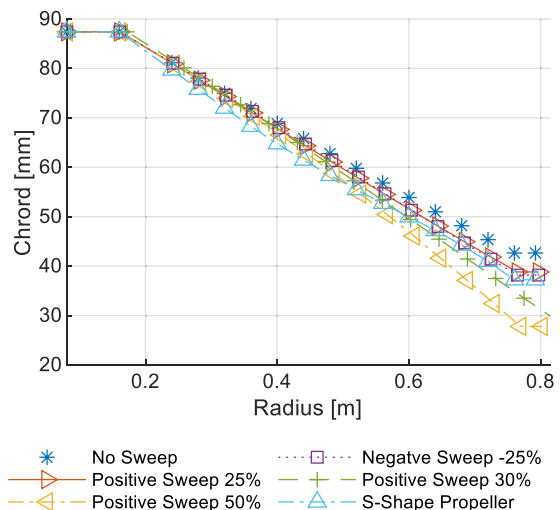


FIGURE 9: Chord distribution of analysed propeller

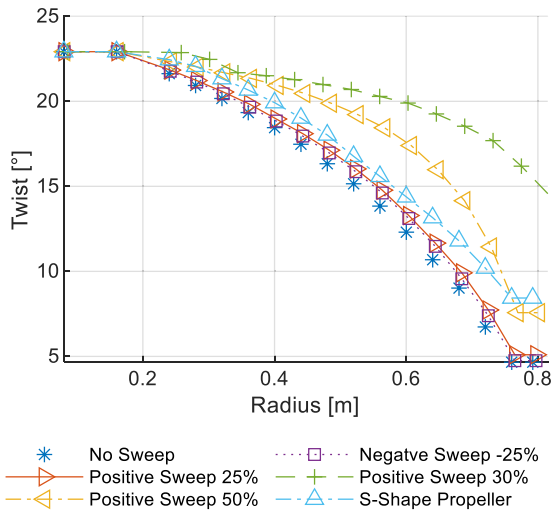


FIGURE 10: Twist distribution of analysed propeller

4. RESULT EVALUATION

First we compare and evaluate the results of the RANS prediction. In a second step, the presented correction steps for BEM methods are compared against the RANS prediction per propeller to find the best matching correction method.

4.1. RANS results

FIGURE 11, FIGURE 12 and FIGURE 13 show the predicted thrust coefficient, power coefficient and efficiency from the RANS simulations.

First, comparing the thrust coefficient difference of the 25% forward and backward swept propeller to the unswept propeller indicates that sweep below 25% has a minor influence on propeller performance. Forward sweep is slightly decreasing thrust while backward sweep is slightly increasing thrust. The comparison of the power coefficient shows that for the 25% swept propellers, the power coefficient of the backward swept propeller is slightly increased. In contrast, a significant power consumption reduction is observed for the forward swept propeller. In total, the efficiency of the 25% swept propeller is not affected.

Second, comparing the increased sweep with 50% backward sweep and the unswept propeller shows a significant change in thrust, power and high J conditions. The strong sweep especially improves the high J region in terms of thrust and efficiency. While the less swept propeller stopped providing thrust, the stronger swept propeller still provide thrust by an acceptable efficiency (compare FIGURE 13).

Third, the s-shape propeller has a similar low J behaviour as the unswept propeller, but the high J performance is strongly improved. As by the 50% swept propeller, the operating region is increased. On the other hand, the power

consumption is significantly increased, resulting in worse efficiency. However, the operating range is improved against the unswept and less swept propeller.

Finally, comparing the 30% propeller with the unswept propeller shows the combined trend of the 50% swept propeller and s-shape propeller. Thrust coefficient is reduced in low J conditions, but higher J conditions are possible. Power consumption is massively increased, resulting in the worst efficiency but a high operational range.

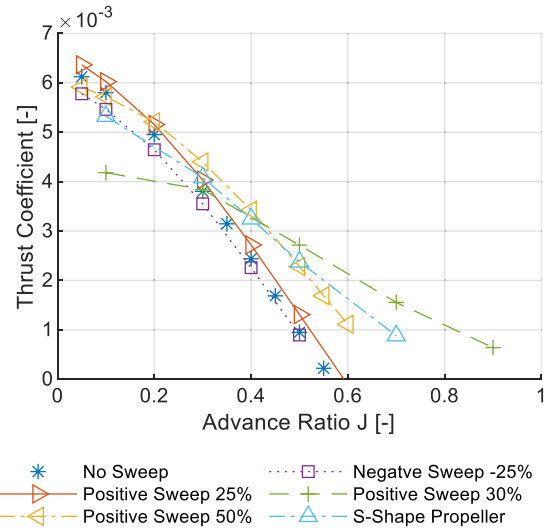


FIGURE 11: StarCCM+: Thrust coefficient comparison

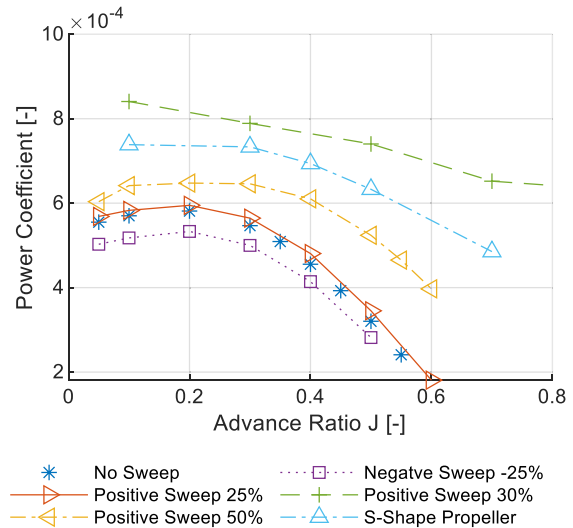


FIGURE 12: StarCCM+: Power coefficient comparison

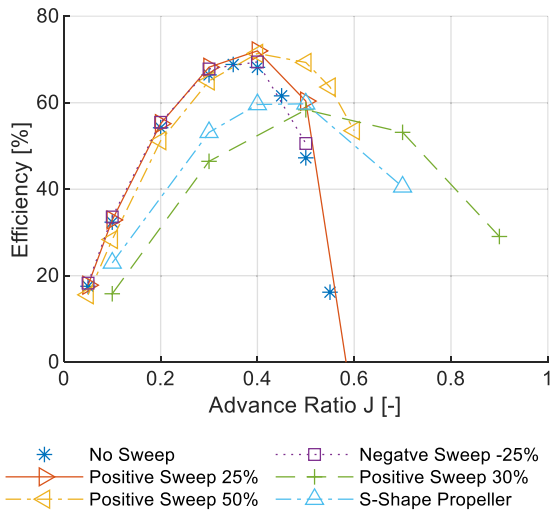


FIGURE 13: StarCCM+: Efficiency comparison

The comparison of the RANS results indicates that no correction model is required for the less swept propeller below 25% sweep. Propeller sweep is increasing the operational range of the propeller to higher J conditions. However, the increased operational range is paid by efficiency.

4.2. RANS and BET Comparison

In this subchapter following correction steps to the classical unswept BET method (step 0) are applied accordingly to subchapter 2.1:

0. **No Correction:** No sweep correction applied. Airfoils cut orthogonal to the global x-axis
1. **Turned:** Turned airfoils without further correction
2. **Lift Correction:** Turned airfoils with lift correction only (equation (17))
3. **Q Correction:** Turned airfoils with lift correction only and turned Q' force (equation (19))
4. **Drag correction:** Turned airfoils with lift and drag correction as well as Q' force correction as a new method (equation (18))

For validation purposes, first the unswept propeller is analysed. Second, the 50% swept propeller is presented in detail, and third, an overview about all analysed propellers is presented. The 50% swept propeller is selected as example, because it shows the correction steps best. However, this strong propeller sweep isn't realistic for executed propellers. Performance curves for the missing propeller are attached in the appendix.

The Validation case in FIGURE 14 and FIGURE 15 shows that thrust prediction with BET methods matches RANS data great for the unswept propeller, while power consumption predictions compared to RANS data has relevant errors in low J conditions. However, the relative error in power consumption in low J conditions is below 10%. The BET method underpredicts the power consumption in high J conditions and isn't matching the trend perfectly.

The comparison of the correction methods shows no significant difference between the uncorrected and corrected methods. Minor changes are present due to the geometric build-up of the propeller. The propeller is staggered at the mid-point, while the BET procedure is evaluating sweep at the quarter chord point. Due to taper, a fraction of local sweep is induced, resulting in minor thrust and power consumption changes.

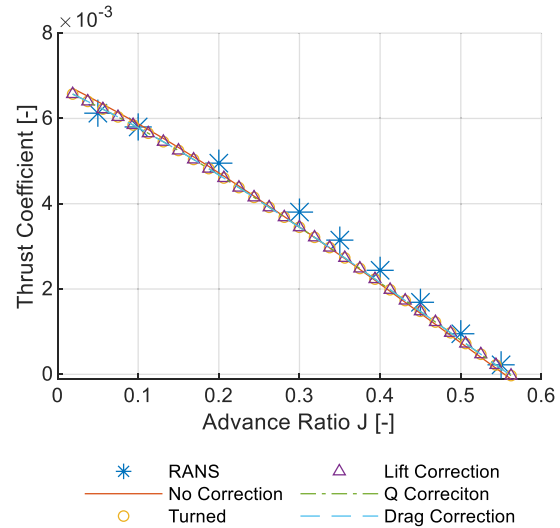


FIGURE 14: No Sweep: Thrust Coefficient

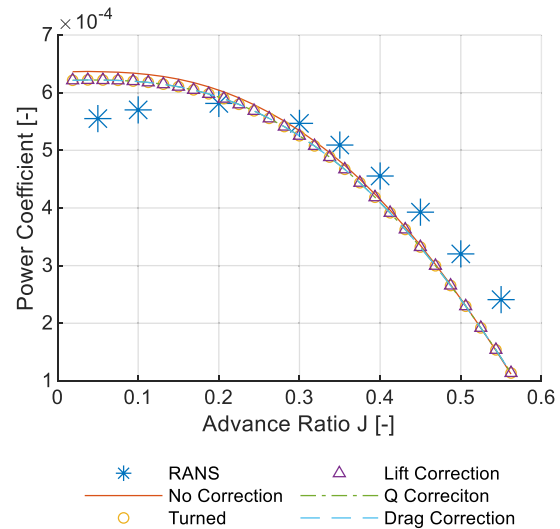


FIGURE 15: No Sweep: Power Coefficient

FIGURE 13 and FIGURE 14 show that the 50% swept propeller has significant differences between the turned and uncorrected procedure. While the uncorrected propeller has no post-stall region for low J, the corrected propeller shows a significant thrust and power consumption breakdown in low J conditions. The angle of attack of the turned airfoils increases due to the changed cutting procedure and the changing twist distribution. The increased twist results in high effective angles of attack in the post-stall region of the 2D airfoil polars. The post-stall is

modelled by the well-known procedure according to Ref. [17]. However, the slope of RANS and BET does not match. RANS predict a reduced slope compared to the BEM methods. The BEM correction methods improve the matching of the slopes, which generally improve the prediction. The example shows the need for turned airfoils for better matching of RANS and BET.

All applied correction methods reduce the predicted thrust and power consumption compared to the unturned airfoils. The novel approach with drag and force directivity correction improves the low J prediction significantly. Thrust is mainly affected by the lift coefficient reduction due to the cosine correlation and the order of lift coefficient compared to drag coefficient (compare equation (9)). The power prediction is also affected by the lift change but also in the same manner by all further corrections.

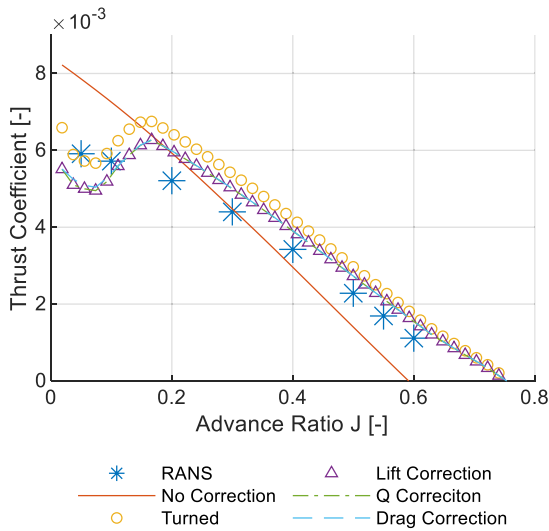


FIGURE 16: 50% Backward Sweep: Thrust coefficient

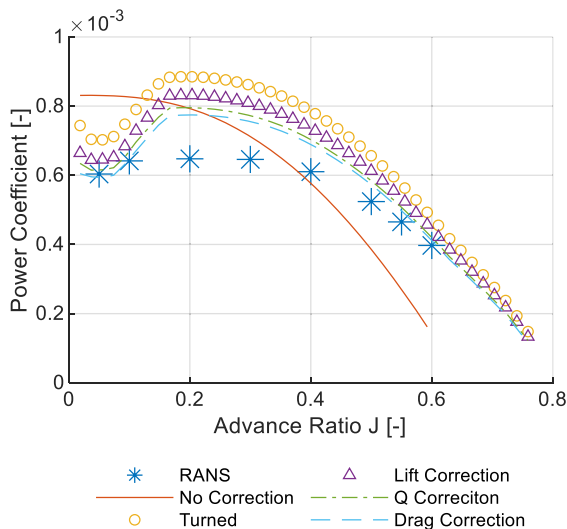


FIGURE 17: 50% Backward Sweep: Power coefficient

To reduce the number of figures, we summarised all results in FIGURE 18 and FIGURE 19. Shown is the difference between the uncorrected and the fully corrected simulation compared to the RANS data. Presented is the improvement of the absolute error as stated in the equation below.

$$(18) \quad C_{\text{Improve}} = \Delta C_{\text{NoCor.}-\text{RANS}} - \Delta C_{\text{DragCor.}-\text{RANS}}$$

Negative values correspond to an increased absolute error, which means the uncorrected BET procedure matches the RANS data better than the corrected BET procedure. High improvements in the plot correspond to significant improvements due to the correction procedure. This approach allows to show improvements but prevent evaluating the overall trend. For evaluate the overall trend, it is necessary to compare the performance curves directly, as shown in the previous figures for the 50% swept propeller. However, this comparison allows evaluating all propeller and correction methods simultaneously.

In general, the prediction is significantly improved in the low J condition. Power and thrust coefficients are improved for all simulations. For the unswept propeller, changes in thrust and power coefficients of 10^{-5} are visible. RANS predicts a slightly different slope than the BET approach resulting in an improvement at low and high J regions and degradation in the mid J region. The sweep correction model enhances the prediction with increased sweep. A significant improvement is already reached for the 25% forward and backward swept propeller. Evaluating the 50% swept propeller shows an alternation between improvement and deterioration. The alternation is explained by the differences in slope between RANS and BET exemplary shown in FIGURE 16 and FIGURE 17. The s-shape and 30% forward swept propeller has significant improvements except in really high J conditions. The slope derivations also explain these outliers between RANS and BET.

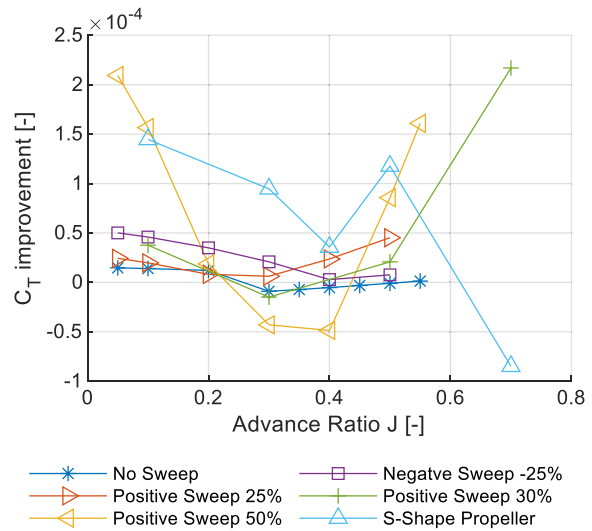


FIGURE 18: Thrust coefficient improvement between uncorrected and fully corrected simulation

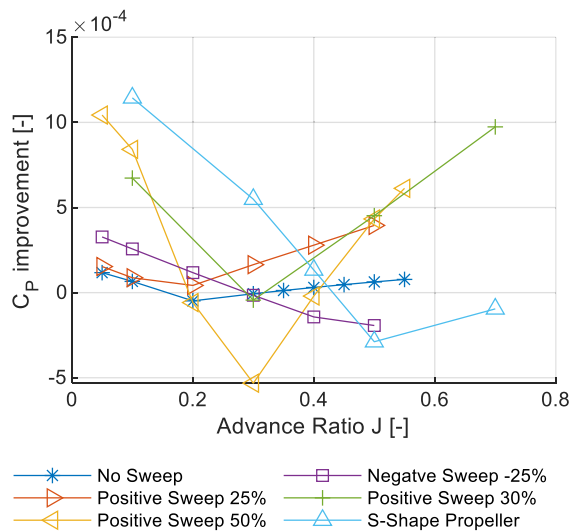


FIGURE 19: Power coefficient improvement between uncorrected and fully corrected simulation

Finally, the novel sweep correction model significantly improves the power consumption prediction compared to the known lift correction model and the uncorrected BET. The sweep correction model is consistently improving the prediction accuracy in trend.

5. CONCLUSION

This paper presents sweep correction models for BET procedures in open propeller analysis. Compared to existing lift correction methods, the novel approach additionally includes drag and tangential force corrections. The local 2D forces are acting in the plane of the incoming airflow. Therefore, we conclude that it's necessary to turn the force back in the local tangential coordinate system. Drag correction is justified by the reduction of the tangential velocity orthogonal to the local sweep. For fixed-wing aerodynamics, this effect might be less pronounced, but in propeller aerodynamics and torque prediction, a significant impact is observed as presented.

For the analysis of the sweep correction models, a generic propeller is created, with the capabilities to change single design parameters with reduced impact on the overall propeller geometry and planform. The comparison of high fidelity RANS data with low fidelity BET simulations for an unswept propeller shows the strength of BET for straight propellers. After further comparison and analysis of forward, backward, and combined swept propeller, the following is conducted:

1. Turning airfoils is crucial for swept propeller analysis and swept propeller description.
2. Up to 25% sweep, BET results fit RANS simulations reasonably well.
3. The lift coefficient correction, according to Busemann, improves the power and thrust prediction significantly.
4. Correction of the tangential force direction and the drag further improves the power consumption

prediction but does not impact the thrust prediction

The authors recommend using the presented approach for all kinds of propeller planforms to improve simulation accuracy.

Further validation of the approach is required using RANS and wind tunnel tests. Additionally, the selected RANS approach is only validated with static test data and the higher resolution rigid body motion RANS approach, as shown in [4]. Further validation with wind tunnel tests is required.

6. REFERENCES

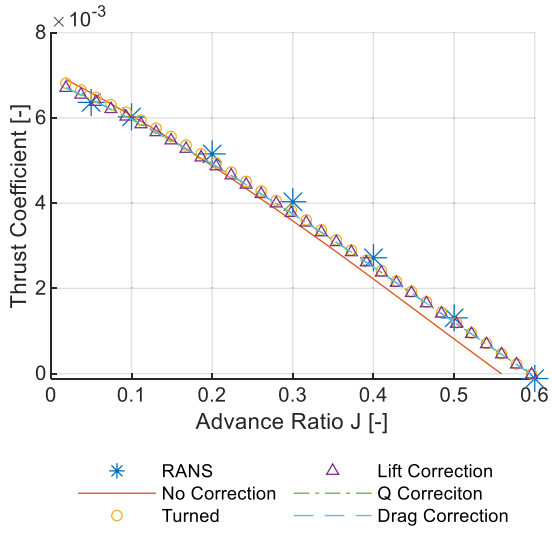
- [1] M. Y. Pereda Albarrán, M. Kreimeier, W. Enders, and E. Stumpf, "Noise evaluation of battery powered small aircraft," *CEAS Aeronaut J.*, vol. 2019, 2019, doi: 10.1007/s13272-019-00404-2.
- [2] S. A. Ning: Brigham Young University and G. Hayman, R. Damiani, and J. Jonkman: NREL, "Development and Validation of a New Blade Element Momentum Skewed-Wake Model within AeroDyn: Preprint,"
- [3] T. Wright and S. E. William, "Blade Sweep for Low-Speed Axial Fans," *ASME Journal of Solar Energy Engineering*, vol. 1989, no. 53.
- [4] O. Bergmann, F. Götten, C. Braun, and F. Janser, "Comparison and Evaluation of Blade Element Methods against RANS Simulations and Test Data," in *DLRK 2020*, Deutsche Gesellschaft für Luft und Raumfahrt, Ed., 2020.
- [5] A. Busemann, "Aerodynamischer Auftrieb bei Überschallgeschwindigkeiten," in *Conference Proceedings*, Volta Congress, Ed., 6th ed., Reale Accademia d'Italia, 1935.
- [6] O. Gur and A. Rosen, "A novel approach to actuator disk modeling," 2007.
- [7] A. Rosen and O. Gur, "Novel Approach to Axisymmetric Actuator Disk Modeling," *AIAA Journal*, vol. 46, no. 11, pp. 2914–2925, 2008, doi: 10.2514/1.37383.
- [8] M. Â. R. Silvestre, J. Morgado, and J. C. Pascoa, "JBLADE: a Propeller Design and Analysis Code," *International Powered Lift Conference*, p. 27, 2013, doi: 10.2514/6.2013-4220.
- [9] F. Mahmuddin, "Rotor Blade Performance Analysis with Blade Element Momentum Theory," in *ICAE 2016*, International Conference of Applied Energy, Ed., 2016, pp. 1123–1129.
- [10] J. Sodja, R. Breuker, D. Nozak, R. Drazumeric, and Marzocca P., "Assessment of low-fidelity fluid–structure interaction model for flexible propeller blades," *Aerospace Science and Technology*, vol. 78, pp. 71–88, 2018, doi: 10.1016/j.ast.2018.03.044.
- [11] A. Stürmer, "Unsteady CFD Simulations of Propeller Installation Effects," *AIAA/ASME/SAE/ASEE Joint Propulsion Conference & Exhibit*, vol. 2006, 42th,

2006.

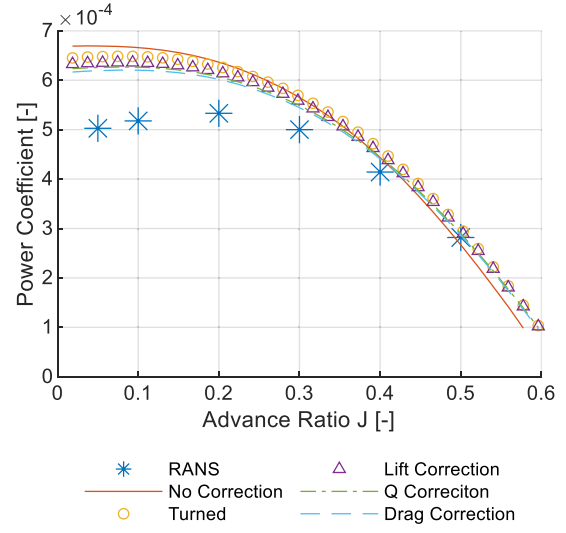
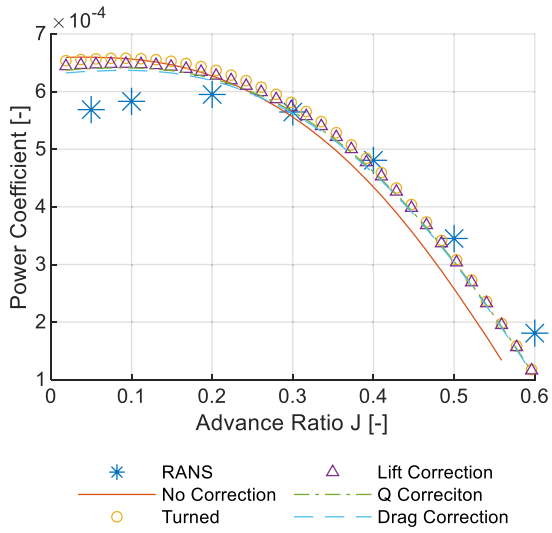
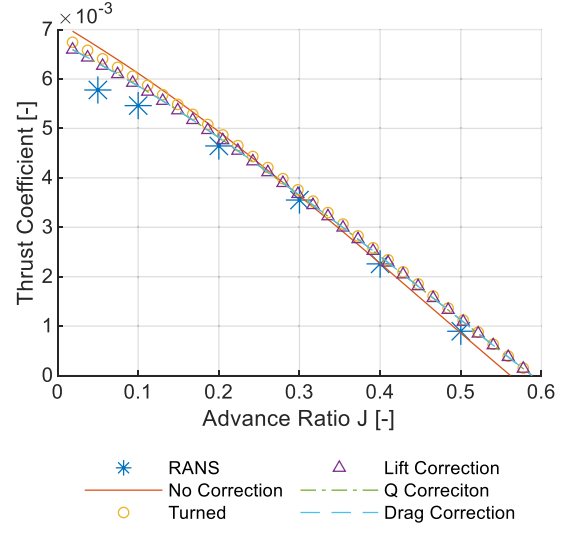
- [12] *Star-CCM+*: Siemens. [Online]. Available: https://documentation.thesteveportal.plm.automation.siemens.com/starccmplus_latest_en/index.html#page/STARCCMP/GUID-86871D8D-72FB-499E-843F-79BD4E0FEFA8.html
- [13] F. R. Menter, "Two-equation eddy-viscosity turbulence models for engineering applications," *AIAA Journal*, vol. 32, no. 8, pp. 1598–1605, 1994, doi: 10.2514/3.12149.
- [14] P. R. Spalart, "Strategies for turbulence modelling and simulations," *International Journal of Heat and Fluid Flow*, vol. 2000, no. 21, pp. 252–263.
- [15] P. R. Spalart and C. L. Rumsey, "Effective Inflow Conditions for Turbulence Models in Aerodynamic Calculations," *AIAA Journal*, vol. 2007, no. 45, pp. 2544–2553.
- [16] Falk Götten, "Exploration and Development of New Drag Prediction Models for UAVs," Doctorial Thesis, RMIT University, Malbourn, 2021.
- [17] D. A. Spera, "Models of Lift and Drag Coefficients of Stalled and Unstalled Airfoils in Wind Turbines and Wind Tunnels," Jacobs Technology, Inc., Oct. 2008.

7. APPEDNDIX

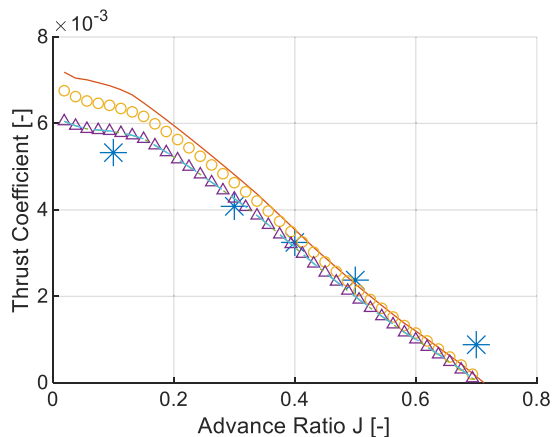
7.1. Positive Sweep 25%



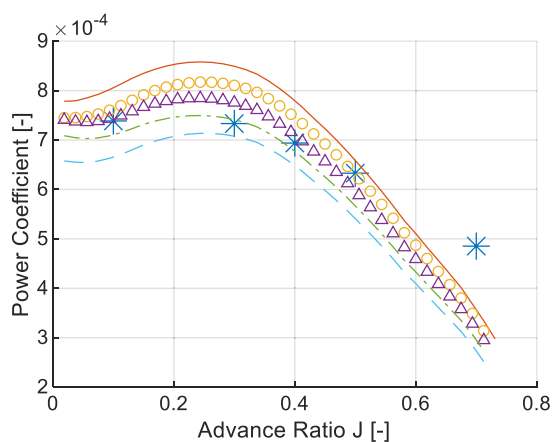
7.2. Negative Sweep 25%



7.3. S-Shape Propeller

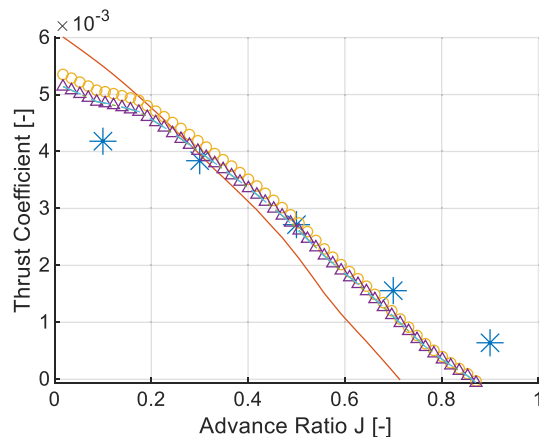


* RANS \triangle Lift Correction
 — No Correction - - - Q Correction
 o Turned - - - Drag Correction

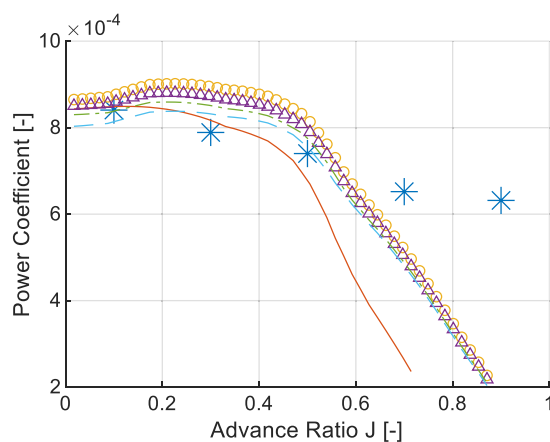


* RANS \triangle Lift Correction
 — No Correction - - - Q Correction
 o Turned - - - Drag Correction

7.4. Positive Sweep 30%



* RANS \triangle Lift Correction
 — No Correction - - - Q Correction
 o Turned - - - Drag Correction



* RANS \triangle Lift Correction
 — No Correction - - - Q Correction
 o Turned - - - Drag Correction